

Large-Eddy Simulation Study on Cycle-to-Cycle Variation of Knocking Combustion in a Spark-Ignition Engine

Ceyuan Chen ^a, Pinaki Pal ^{b,*}, Muhsin Ameen ^b, Dengquan Feng ^a, Haiqiao Wei ^{a,*}

^a State Key Laboratory of Engines, Tianjin University, Tianjin 300072, P. R. China

^b Energy Systems Division, Argonne National Laboratory, Lemont, IL, USA

Submitted to: **Applied Energy**

**Corresponding authors: E-mail address: whq@tju.edu.cn
E-mail address: pal@anl.gov*

Abstract

The cycle-to-cycle variation in the knock intensity is commonly encountered under the abnormal combustion conditions. The severity of these abnormal combustion events can vary significantly, and the efficiency of engines at high loads is limited in practice by heavy knocking phenomena. Since, a thorough analysis of such recurrent but non-cyclic phenomena via experiments alone becomes highly cumbersome, in the present work, a multi-cycle large-eddy simulation study was performed to quantitatively predict cyclic variation in the combustion process and cyclic knock intensity variation in a direct-injection spark-ignition engine. To account for the turbulence-chemistry interaction effects on flame propagation, the G-equation combustion model was used. Detailed chemistry was solved outside the flame front with a toluene primary reference fuel skeletal kinetic mechanism. For both the mild knock and heavy knock conditions, the numerical results were validated against experimental measurements. Based on the simulation results, a correlation analysis was performed considering combustion phasing, peak cylinder pressure and maximum amplitude of pressure oscillation. Furthermore, a detailed three-dimensional spatial analysis illustrated the evolution of auto-ignition kernel development and propagation of pressure waves during knocking combustion for three typical cycles with different knock intensities. It was found that an early occurrence of auto-ignition in the end gas was prone to high knock intensity. Although multiple auto-ignition kernels were observed in different cycles, the degree of coupling between chemical heat release and pressure waves varied, thereby leading to different maximum amplitude of pressure oscillation values.

Keywords: Engine Knock; Cycle-to-cycle Variation; Auto-ignition; Pressure Oscillation, Large-Eddy Simulation

1. Introduction

The transportation sector is a key component of the modern global economy and accounts for around 20% of the energy consumed worldwide [1]. This global demand is only going to rise in the foreseeable future. At present, almost the entire global transport is powered by combustion engines, burning liquid petroleum fuels. On the other hand, the transportation sector is responsible for 14% of global greenhouse gases (GHG) including CO₂ emissions [2]. Therefore, in view of growing environmental concerns, stringent emission regulations on vehicle fuel consumption and emissions have been mandated in many countries. In order to meet these regulations, the efficiency and fuel economy of vehicle powertrains needs to be improved.

At present, around 85% of the 1.1 billion passenger cars in the world are powered by gasoline SI engines. Moreover, the daily global demand for gasoline is approximately 4.7 billion litres, which accounts for nearly 40% of the demand for global transport energy [3]. Engine downsizing coupled with boosted operation is considered an attractive strategy to enhance power density and reduce fuel consumption of SI engines [4]. However, these operating conditions result in severe thermodynamic conditions, thereby promoting the likelihood of abnormal combustion phenomena such as knock [5] and super-knock [6]. Knocking refers to the sharp metallic noise that occurs as a result of premature auto-ignition of the end-gas mixture ahead of the propagating flame front in a SI engine [7]. This leads to rapid heat release and high-frequency pressure oscillations, which are severely detrimental to engine durability. As a result, knock imposes stringent constraints on the high-load performance and efficiency of SI engines by prohibiting the use of more advanced spark timings, higher compression ratios and higher boost pressures[8] . On the other hand, knock is intertwined with the local thermal and mixture stratifications in the in-cylinder flow field, which makes it a recurrent but non-cyclic phenomena.

Due to the possible destructive characteristics and associated cycle-to-cycle variation (CCV), experimental study of knocking combustion has its limitations. With the ability to isolate the effects of certain factors (such as state of the unburnt mixture, complex chemical kinetics and turbulence-chemistry interaction (TCI) [9]) which are strongly coupled with each other during knock and elucidate much more details of the knocking phenomena, computational fluid dynamics (CFD) is considered a viable complement to experiments. The pioneering works of Zel'dovich [10] and Gu et al. [11] quantified different reaction front propagation modes originating from an auto-ignition (AI) kernel surrounded by a non-uniform distribution of chemical reactivity. Five propagation modes with different flame propagation speeds and degrees of coupling between pressure wave and flame front were identified: thermal explosion, supersonic auto-ignitive deflagration, developing detonation, subsonic auto-ignitive deflagration, and normal flame deflagration. More recently, non-dimensional regime diagrams were also proposed to quantify weak and strong ignition regimes, incorporating the effects of turbulence, chemistry and thermal inhomogeneities [12, 13]. The 1-D simulations conducted by Dai et al. [14] presented different AI modes in a simplified configuration, and they were summarized in terms of the normalized temperature gradient and acoustic-to-excitation time scale ratio. The results showed that the negative temperature coefficient (NTC) characteristics of surrogate fuels had no obvious effect on the transition between AI modes. However, the 1-D numerical study of Terashima et al. [15] revealed that NTC behavior influences the timing of the pressure oscillation during knock. Apart from the investigations on single initial AI spot, the interaction between AI spots has also been studied [16]. Wei et al. [17] showed that a detonation wave could generate within the limited end gas region with multi-AI spot interaction. Furthermore, the effect of turbulence on spontaneous ignition has been explored. The DNS study of Yoo et al. [18, 19] showed that with intensive turbulent mixing, the auto-ignition

process of *n*-heptane/air mixture was retarded, but leads to a more rapid and homogeneous auto-ignition. Wei et al. [9] integrated LES and 1-D stand-alone LEM (linear eddy mixing model) to investigate the effect of turbulence on the formation and development of AI kernels. The results revealed that high turbulent motion results in a prolonged ignition delay. Furthermore, the initial scale of the AI kernel decreased with an increasing turbulent intensity, and strong turbulent mixing changed the combustion mode of end gas auto-ignition under a low initial mixture temperature (below the NTC regime).

Over the last few decades, 3-D engine CFD modeling has been extensively used to gain a better understanding of knocking phenomena. A hybrid combustion modeling technique coupling the finite-rate chemistry and G-equation approaches was developed to capture knock by Liang et al. [20]. Pal et al. [21] employed this methodology along with a tabulated laminar flame speed approach to predict knocking combustion of multi-component gasoline fuel surrogates in a Cooperative Fuel Research (CFR) engine. Netzer et al. [22] utilized the same combustion model and coupled engine CFD simulations with detonation theory [23] to quantify the severity of end-gas auto-ignition. Notably, unsteady RANS framework was used in these previous works, which were primarily focused on the effects of fuel composition and/or operating condition on averaged knock tendency rather than the link between knock and CCV. D'Adamo et al. [24] proposed a statistically based RANS knock model to predict both ensemble averaged knock occurrence and knock probability from engine CFD simulations.

Due to the capability of capturing unsteady flow features more accurately than RANS, LES is considered a promising tool [25] to capture CCV under practical conditions. Robert et al. [26] demonstrated, for the first time, an LES methodology using ECFM (extended coherent flamelet model) [27] and TKI (tabulated kinetics of ignition) combustion models [28], to quantitatively describe knocking combustion in a boosted homogeneous SI engine configuration. The dependency of knock

tendency on spark timing (ST) was analyzed; numerical simulations were able to provide reasonable prediction of in-cylinder pressure variability, knock occurrence frequency and mean knock onset crank angle. The simulation data was further analyzed to understand the end gas auto-ignition phenomena at different operating conditions. However, both these studies were performed for iso-octane (with octane sensitivity of zero and Research Octane Number (RON) of 100), which is not representative of the chemical kinetics of practical gasoline fuels. Moreover, in order to speed up the simulations with different STs, the LES consecutive cycles with a reference ST were used to provide independent initial conditions, and only the combustion phases of each cycle were simulated by changing the ST. Although this methodology was employed to simulate a wide range of knocking behaviors, the simulations were validated against experiments for low to moderate knock intensities (up to 2 bar) only. Pan et al. [29] investigated engine knock and super-knock in a port fuel injected (PFI) engine using a LES framework coupling detailed chemistry solver, thereby not accounting for TCI effects on flame propagation. Moreover, only closed-cycle LES were performed for different STs, binary primary reference fuel (PRF) surrogates were considered, and a rigorous validation of the knock metrics predicted by simulations was not performed. More recently, Robert et al. [30] conducted an analysis of knock for a direct-injection spark-ignition (DISI) engine using the same LES methodology as used in previous works [39, 40]. Although a more realistic three-component TPRF surrogate was used for gasoline, this study was limited to light knocking conditions (knock intensity ≤ 1 bar).

In the context of the above discussion, the present work extends the state-of-the-art in numerical modeling and analysis of knock CCV under practical engine conditions. In contrast to previous studies, a more comprehensive numerical investigation is performed which simultaneously incorporates the following: (a) consecutive-cycle engine LES, (b) practical DISI conditions (exhibiting both thermal

and mixture stratifications), (c) modeling of TCI effects on flame propagation, (d) realistic multi-component TPRF surrogate to represent practical gasoline fuel, and (e) wide range of knock intensities with rigorous model validation against experimental data. In particular, multi-cycle LES was performed under mild knock and heavy knock conditions of a single-cylinder DISI engine. LES results were compared with experimental data with respect to a variety of knock metrics for model validation. A correlation analysis was performed among combustion phasing, peak cylinder pressure and maximum amplitude of pressure oscillation (MAPO). Moreover, the relationship among MAPO, magnitude of flow velocity and standard deviation of flow velocity near the spark plug close to the ignition timing was investigated. The mechanisms that lead to high and low knock intensity (KI) were analyzed, and the interaction between combustion variability and cyclic changes in the flow patterns was analyzed.

The remainder of the paper is organized as follows. The experimental setup and numerical approach are described in sections 2 and 3, respectively. Then, based on the LES results, the knocking combustion process of multiple cycles is presented and analyzed in section 4. Finally, the major conclusions are drawn in the last section.

2. Experimental setup

Table 1 Characteristics of the engine bench and operating conditions.

Engine type	Single cylinder, 4-stroke
Fuel	Commercial Gasoline #92
Bore×Stroke	80×100 mm
Sweep volume	0.5 L
Compression ratio	10.0:1
Connecting Rod	185.0 mm

Valve mechanism	overhead camshafts, 2-valve
DI injector	Siemens piezoelectric injector
DI pressure and SOI timing	20.0 MPa, 240.0 bTDC
Speed	1500.0 r/min
Spark Timing	20.0, 22.0 CAD bTDC
Intake valve Open / Close timing	380.0 bTDC / 140.0 bTDC
Exhaust valve Open / Close timing	580.0 bTDC / 340.0 bTDC

A single-cylinder, four-stroke DISI engine (Ricardo E6) was used as the experimental test bench.

The geometry is simple with a flat piston and pent-roof combustion head, making it easy to define the boundary conditions. The fuel injector is a Siemens VDO piezoelectric pintle injector. The injection pressure was 20.0 MPa with start-of-injection (SOI) timing of 120.0 bTDC (during the intake process).

The overall equivalence ratio of the air/fuel mixture was measured by a wideband lambda sensor with an uncertainty of $\pm 0.8\%$. To achieve a stoichiometric mixture, the DI injection timing, pressure and duration were adjusted by using the in-house programs developed in the LabVIEW software. A direct current dynamometer was coupled with the engine to maintain a constant speed of 1500 r/min, with an accuracy of ± 1 r/min. The ST was controlled by MOTEC ECU: 20.0 CAD bTDC and 22.0 CAD bTDC were adopted. The characteristics of the engine bench and operating conditions are summarized in Table

1.

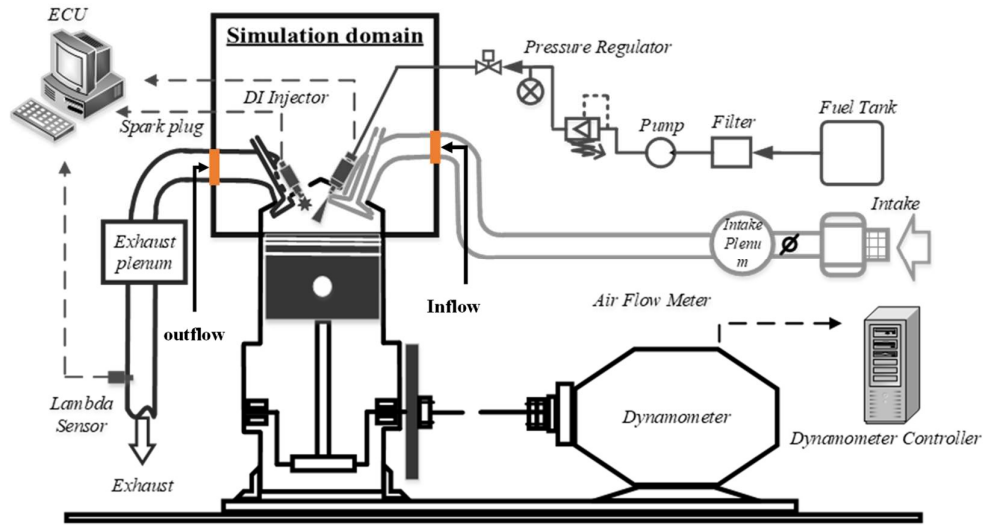


Fig.1. A schematic of the experimental test bench.

In-cylinder pressure data was acquired by a flat mounted water-cooled piezoelectric pressure transducer (Kistler 6041A). The charge signal amplifying and recording were performed by a Kistler 5018 charge amplifier and a National Instruments PC-6123 data acquisition card. Pressure sampling was triggered using a digital encoder coupled to the crankshaft with a resolution of 0.1 CAD. The scale of the adopted fuel meters ranged from 0 to 125.0 kg/h with the uncertainty of $\pm 0.2\%$. Coolant and oil temperatures were controlled by a SIEMENCE proportional-integral-differential (PID) controller with an uncertainty of ± 3 K. Details of the engine setup are shown in Fig. 1.

3. Numerical approach

The geometry adopted in the present LES is shown in Fig. 2. The location of the pressure sensor was the same as that in the experimental setup. The profiles of the intake and exhaust temperatures/pressures were obtained from GT-Power [31]. The in-cylinder pressure trace calculated by GT-Power was validated by comparing with the mean pressure of 199 consecutive cycles from the experiment. Other than temperature and pressure, the Neumann boundary condition was adopted for the other scalars (such as species density, turbulence intensity, etc.). Temperatures of the combustion

chamber boundaries were set according to the conjugate heat transfer (CHT) study of Leguille et al. [32] on the surface temperature distribution in a SI engine under operating conditions similar to the present study. These details are provided in Table 2.

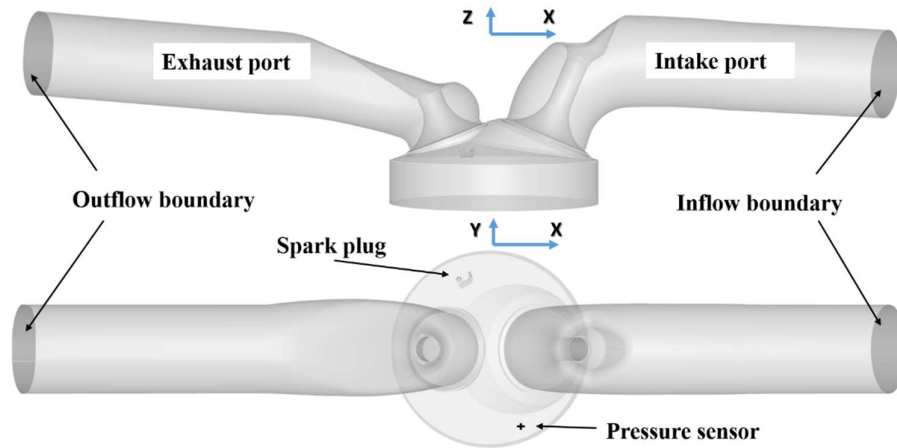


Fig. 2. Engine geometry for 3-D CFD simulations.

The numerical study was performed using a commercial 3-D CFD code, CONVERGE (version 2.3) [33]. The governing equations (conservation of mass, momentum, species and energy) were discretized by a second-order scheme in space and a first-order scheme in time. A conventional Eulerian-Lagrangian Discrete Droplet Model (DDM) [33] was used to model the spray. The liquid spray was modeled as dispersed phase in the Lagrangian framework and the surrounding air was modeled as a continuous phase in the Eulerian framework. The Kelvin-Helmholtz (KH)-Rayleigh-Taylor (RT) spray break-up model [34] was adopted to model droplet break-up and atomization. The No Time Counter (NTC) model [35] was used to simulate the collision outcomes. The injector consisted of 6 nozzles, and no discharge coefficient model was adopted in this study. The duration of injection was determined by matching the measured fuel pressure.

Table 2 Temperatures of the combustion chamber boundaries.

Boundary	Temperature (K)
----------	-------------------

Piston top	450.0
Head	500.0
Cylinder linear	450.0
Exhaust valve bottom	610.0
Exhaust port angle	525.0
Intake valve bottom	550.0
Intake port angle	425.0

The well stirred reactor or SAGE model adopted in the CONVERGE doesn't take the turbulence-chemistry interaction (TCI) into consideration implicitly [36]. Hence, fine grid scale is needed to capture the subgrid-scale effects. However, it makes the simulation unaffordable in term of the computation time. In our previous work [37], the results calculated by SAGE (well stirred reactor) and G-equation were compared to show the advantage of G-equation model when integrated with engineering LES. So, G-equation is still adopted as the turbulent combustion model in the present work. The parameter G is a passive scalar, which represents the distance to the flame front. Inside the flame front, the G value is positive, while outside the flame front it is negative. The flame front has the value of G equal to zero. The turbulent flame front is tracked by solving the transport equation for G passive:

$$\frac{\partial \rho \tilde{G}}{\partial t} + \frac{\partial \rho \tilde{u}_i \tilde{G}}{\partial x_i} = -\rho D_t' \tilde{k} \frac{\partial}{\partial x_i} \left[\frac{\partial \tilde{G}}{\partial x_i} \right] + \rho_u S_t \left[\frac{\partial \tilde{G}}{\partial x_i} \right], \quad (1)$$

where u_i is instantaneous velocity, ρ is the density of the cell, and D_t represents the turbulent diffusion. $\tilde{\cdot}$ stands for the Favre filtering, ρ_u is the unburned density, k is the turbulent kinetic energy. The turbulent flame speed, S_t is calculated as:

$$S_t = S_l \left(-\frac{b_3^2 C_s \Delta x}{2b_1 S_c l_F} + \sqrt{\left(\frac{b_3^2 C_s \Delta x}{2b_1 S_c l_F} \right)^2 + \frac{b_3^2 D_t}{S_l l_F} + 1} \right), \quad (2)$$

where S_l is the laminar flame speed, b_1 and b_3 are modeling constants, C_s is the dynamic Smagorinsky

number, Sc is the turbulent Schmidt number. As shown, the filter size, Δx would affect the sub-grid burning velocity including kinematic restoration and dissipation. Also, with a larger b_l value, the turbulent flame increases monotonously, which makes b_l a straight forward tuning parameter. In this study, the value of 8 is adopted for b_l . The Metghalchi and Keck correlation [38] was adopted in this study to calculate the instantaneous laminar flame speed:

$$S_l = S_{l-ref} \left(\frac{T_u}{T_{u-ref}} \right)^\gamma \left(\frac{P}{P_{ref}} \right)^\beta (1 - 2.1Y_{dil}), \quad (3)$$

where T_u is the unburnt mixture temperature, T_{u-ref} is 298.0 K. P is the unburnt mixture pressure, P_{ref} is 1.01 bar. γ and β are the exponents for temperature and pressure, respectively. Y_{dil} is the mass fraction of the dilution species. S_{l-ref} is obtained by:

$$S_{l-ref} = B_m + B_2(\varphi - \varphi_m)^2, \quad (4)$$

where φ is the equivalence ratio. The recommended modeling constants, B_m (0.2632), B_2 (-0.8472), and φ_m (1.13) for iso-octane were used [33, 38].

Compared with compression ignition engines or engines fueled with alternative fuels, gasoline is still the major energy source for passenger cars [39]. To describe the end gas auto-ignition, finite-rate chemistry model was employed outside the flame front. A toluene primary reference fuel (TPRF) mechanism consisting of 56 species and 168 reactions [40] was adopted to represent the fuel chemistry. The surrogate fuel for the commercial gasoline #92 was chosen to be a TRPF blend with RON = 92, MON = 82 (anti-knock index, AKI = 87). The mass fractions of *n*-heptane (11.8%), *iso*-octane (19.9%) and toluene (68.3%) in the surrogate were obtained by the method proposed by Morgan et al. [41].

Table 3 Mesh size with different embedding and AMR levels.

Refinement method	Level	Mesh size (mm)
Base mesh size	/	4.0
AMR (V&T)	3	0.5

Embedding in cylinder	2	1.0
Embedding in injection	3	0.5
Embedding near spark plug	5	0.125
Embedding near liner	3	0.5
Embedding near piston	3	0.5
Embedding near intake angle	3	0.5
Embedding near exhaust angle	2	1.0

The base mesh size was 4.0 mm. A flexible grid scaling method consisting of fixed embedding (grid size different from the base grid could be specified at a certain location) and adaptive mesh refinement (AMR) was adopted. The grid resolution near the intake valves was 0.5 mm. The grid size inside the cylinder was 1.0 mm. To ensure a good prediction of the spark ignition phenomena, the grid scale near the spark plug gap was 0.125 mm. Velocity AMR was activated in the intake ports and cylinder with the threshold gradient value of 0.25 m/s. Based on our previous study [37], to well predict the combustion process, an AMR based on the reaction progress variable passive, C was activated from ignition to EVO. The progress variable C was transported by solving:

$$\frac{\partial \rho \tilde{C}}{\partial t} + \frac{\partial \rho \tilde{u}_i \tilde{C}}{\partial x_i} = \frac{\partial}{\partial x_i} \left(\rho D_t \frac{\partial \tilde{C}}{\partial x_i} \right) + \rho S, \quad (5)$$

where C equals to 0 in unburnt and burnt mixture without chemical reactions, and becomes equal to 1 when complete combustion occurs. A summary of the various grid scales with corresponding embedding levels adopted in this study is provided in Table 3.

Lastly, to accurately capture the local in-cylinder pressure oscillation during knock, the mach Courant-Freidrich-Lewy (CFL) number, CFL_{mach} was set to 1.0 during combustion.

4. Results and Discussion

For both of the ignition timings, 16 consecutive cycles were simulated with LES. The first cycle was discarded from the analysis as it was affected by the initial conditions. The methodology for simulating the spark timing sweep involves two main steps: first, calculate the 16 consecutive LES cycles with CFL_{mach} of 10; second, re-calculate all the 15 cycles (without the first cycle) from the crank angle just before spark ignition to 60 CAD aTDC with CFL_{mach} of 1. In this way, we could simultaneously accelerate the simulations and obtain accurate results considering the effect of cyclic variation of flow and composition fields on the combustion process. For each LES, 96 processors were used. All the simulations were performed on Blues, a high performance computing (HPC) cluster at Argonne national laboratory. In total, approximately 0.4 million CPU hours were used.

4.1. Model validation

Figure 3 compares the local pressure traces of 199 cycles from experiment (grey lines) and 15 cycles predicted by LES (colored lines) under both the mild and heavy knock conditions. The purple open circles represent the peak pressures and the corresponding crank angles of the experimental cycles. As shown, the experimental pressure envelope is well reproduced by the LES. However, under the heavy knock condition, the three highest pressure peaks are not seen within the 15 cycles at the location of the pressure sensor, and a misfire cycle is encountered in the simulation.

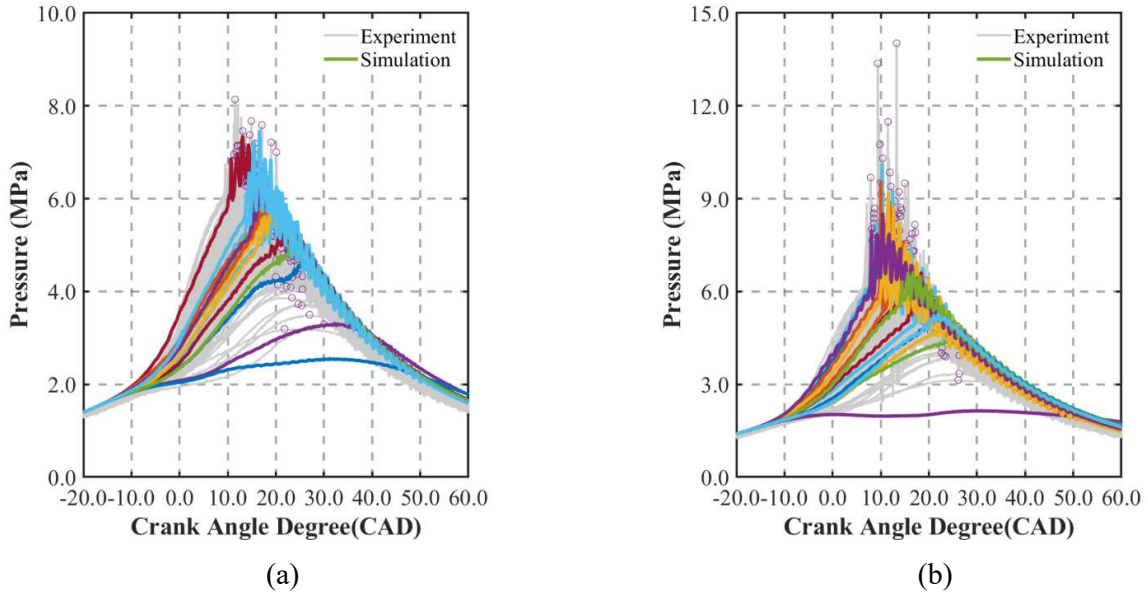


Fig. 3. In-cylinder pressure comparison between experimental and simulation results under the (a) ST = 20.0 bTDC, mild knock condition and (b) ST = 22.0 bTDC, heavy knock condition.

Table 4 Knock relevant indicators comparison between experiment and simulation under the mild knock (ST = 20.0 bTDC) and heavy knock (ST = 22.0 bTDC) conditions.

	θ_{onset} ave (CAD)	θ_{onset} std (CAD)	MAPO ave (MPa)	MAPO cov (/)	θ_{KI} ave (CAD)	θ_{KI} std (CAD)
Exp. 20. CAD	15.0	2.6	0.43	0.50	16.2	2.6
Sim. 20 CAD	16.1	2.5	0.45	0.41	17.9	2.1
Exp. 22 CAD	12.2	3.0	0.87	0.72	14.0	2.8
Sim. 22 CAD	11.9	4.2	1.00	0.76	14.0	4.0

To further analyze the ability of LES to predict knock intensity and cyclic variation of combustion, the averaged value and coefficient of variation (COV) of the knock relevant indicators are compared between experiment and simulation in Table 4. A band-pass filter (2-20 kHz) was applied to the in-cylinder pressure traces. The knock intensity was quantified by the maximum amplitude of pressure oscillation (MAPO) [5]. A cycle was considered to be knocking if the corresponding MAPO exceeded

0.1 MPa. θ_{onset} and θ_{KI} are the crank angles corresponding to the onset of knocking combustion and peak pressure, respectively. In Table 4, “ave” means averaged value, “std” is short for standard deviation. As shown, the LES results agree well with experimental data in terms of both the averaged values and CCV degrees.

4.2. Correlation analysis

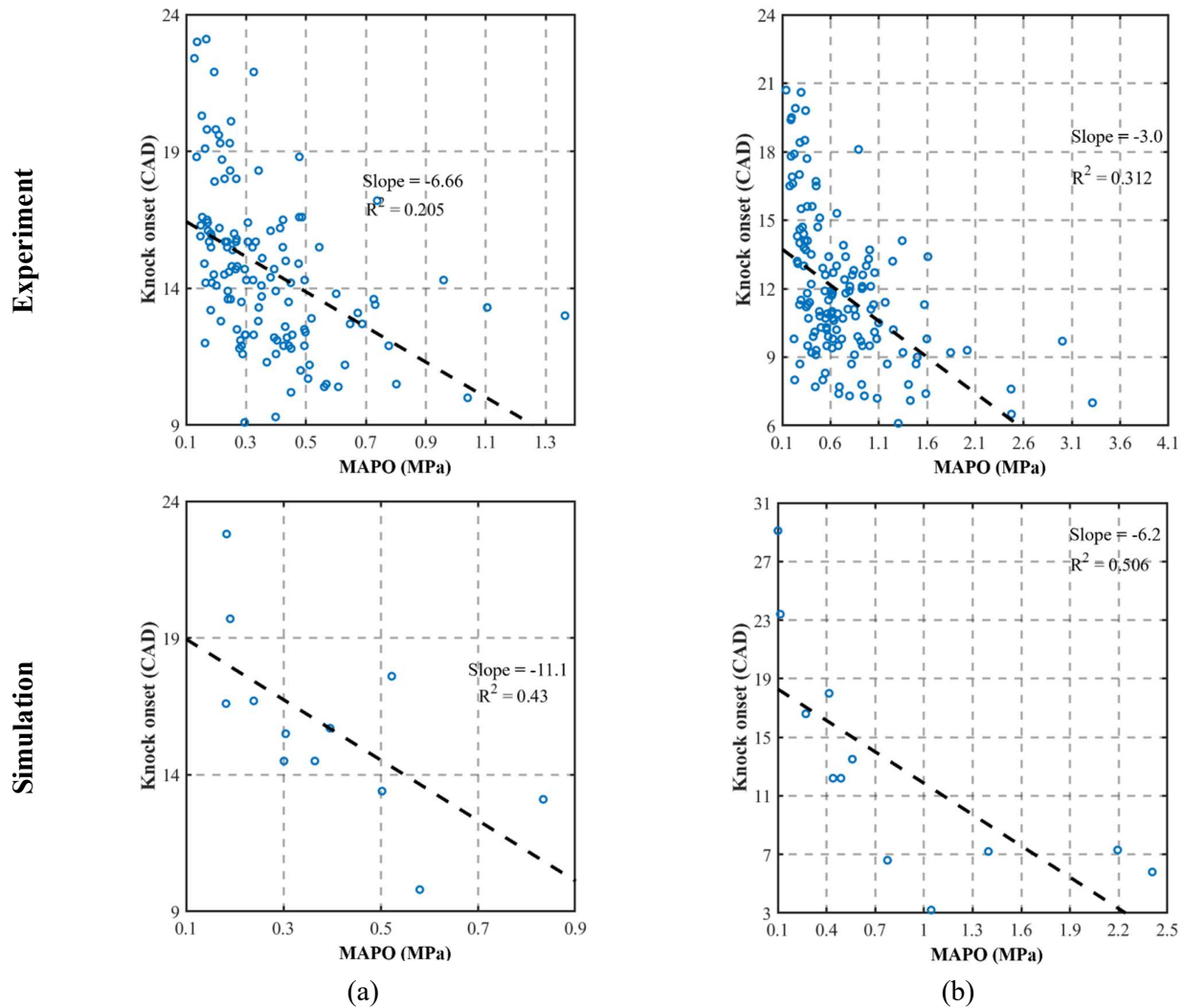


Fig. 4. Correlation analysis on MAPO - θ_{onset} under the (a) mild knock and (b) heavy knock conditions based on experimental data and simulation results.

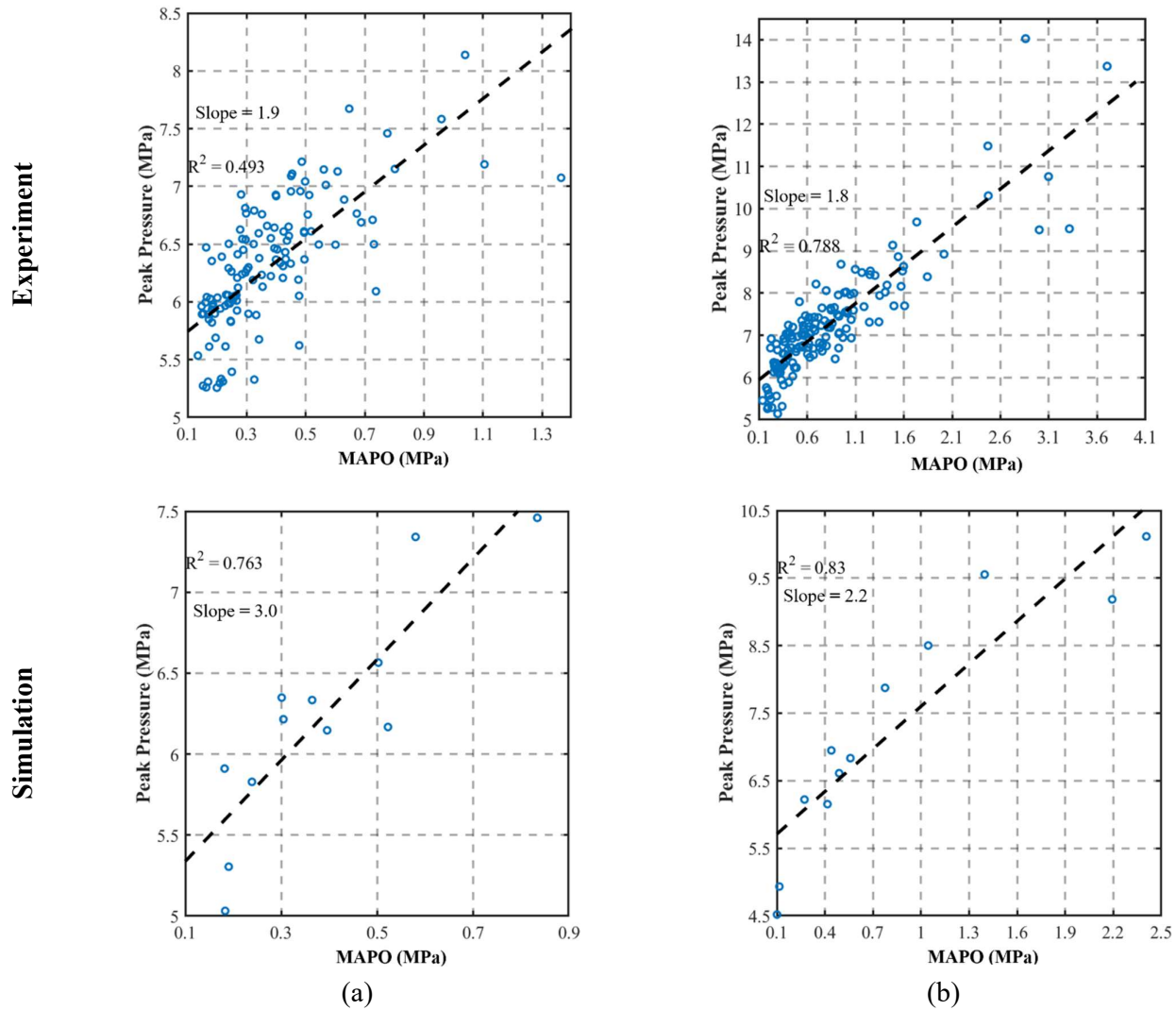


Fig. 5. Correlation analysis on MAPO - Peak pressure under the (a) mild knock and (b) heavy knock conditions based on the experimental data and simulation results.

By conducting the correlation analysis, we aimed to illustrate the relationship between MAPO (knocking intensity) and combustion phasing, peak pressure. The correlation analysis could reveal the physical phenomenon which are inter-related. For example, in our previous simulation work on the normal combustion cycle, the inflow pattern near the ignition timing was shown to have an influence on the early development of ignition kernel, and the change in CA10 affected the IMEP consequently [37].

Figure 4 compares the results of correlation analysis on MAPO and onset of knock between experiments and simulations under both the knocking conditions. As shown, an early occurrence of pressure oscillations is more prone to generate high knock intensity. The negative correlation between knock onset and MAPO is slightly overestimated by the LES, however, the trend illustrated by the experiment that under the heavy knock condition, the correlation coefficient becomes larger, is reproduced by the simulation. It must be noted that only the cycles with MAPO larger than 0.1 MPa were identified as knocking cycles and used for the correlation analysis.

On the other hand, as shown in Figure 5, the correlation between the peak pressure and MAPO is much more obvious. Generally, the cycle with more intensive pressure oscillations has a higher peak pressure, and this positive correlation is stronger under the heavy knock condition. Once again, the reliability of LES has been validated.

Although it is not straightforward to calculate the heat release rate based on the unsmooth in-cylinder pressure trace during abnormal combustion process [42], LES provides a convenient way to analyze the correlation between combustion phasing and knock intensity. The cycle-to-cycle combustion variability can be quantified by various parameters, such as peak pressure and combustion phasing related parameters (CA10 (10% mass fraction burn point) and CA50 (50% mass fraction burn point)). As illustrated in Fig. 6, faster flame propagation tends to generate higher knock intensity. However, this trend depends on the operating condition and geometry of combustion chamber as discussed in Ref. [43].

Figure 7 shows the magnitude and standard deviation of flow velocity in a sphere of 5 mm around the spark plug at -25 CAD bTDC, which is close to the ignition timing. As apparent from Figure 7(a), MAPO has a positive correlation with U_x (x-component of velocity) and its standard deviation. Here,

x-axis denotes the direction from intake valve to exhaust valve as shown in Fig. 2. This observation is in agreement with Robert. et al. [30]. However, under the heavy knock condition which is presented in Fig. 7(b), this relationship is not so obvious.

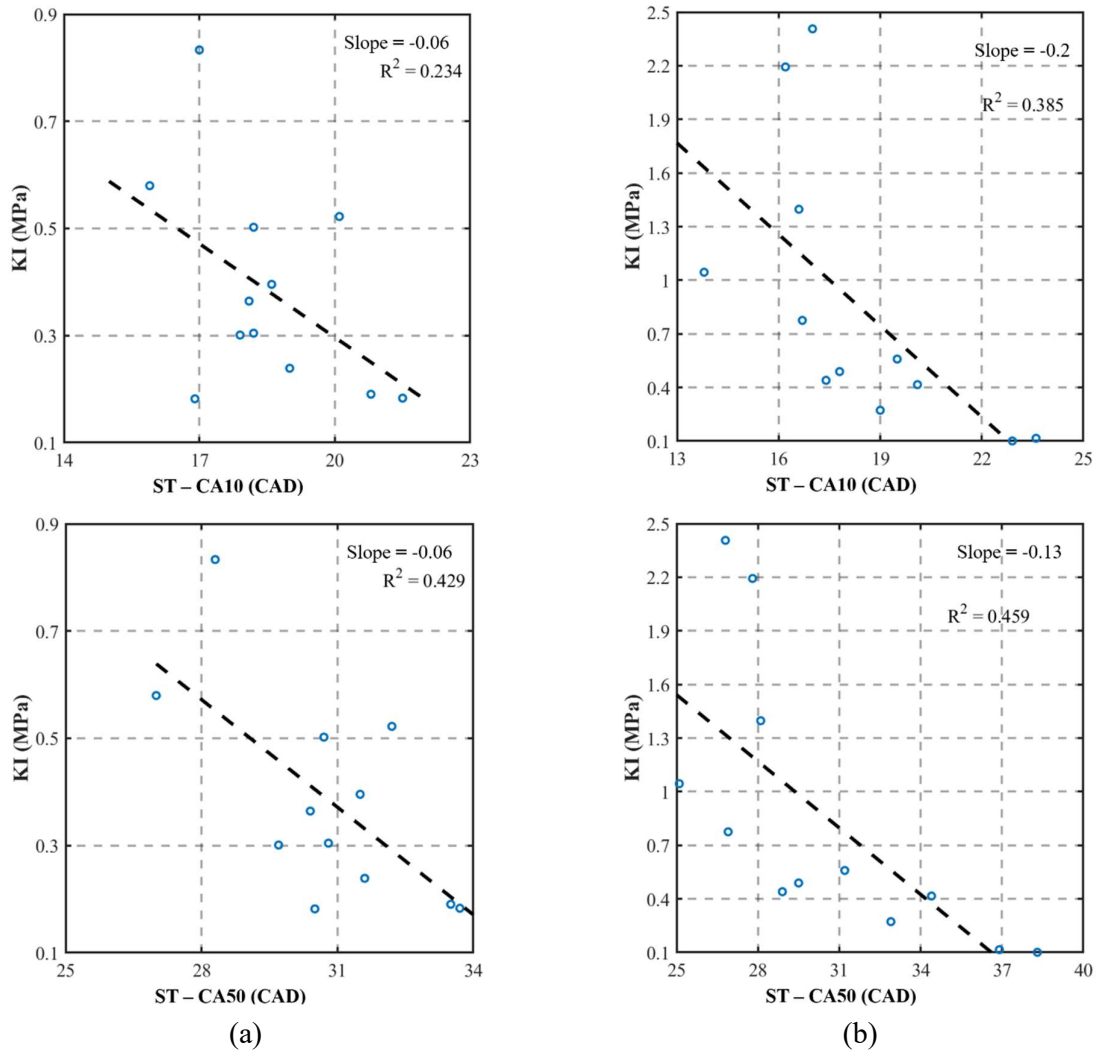


Fig. 6. Correlation analysis on MAPO vs ST-CA10 and MAPO vs ST-CA50 under the (a) mild knock and (b) heavy knock conditions based on LES results.

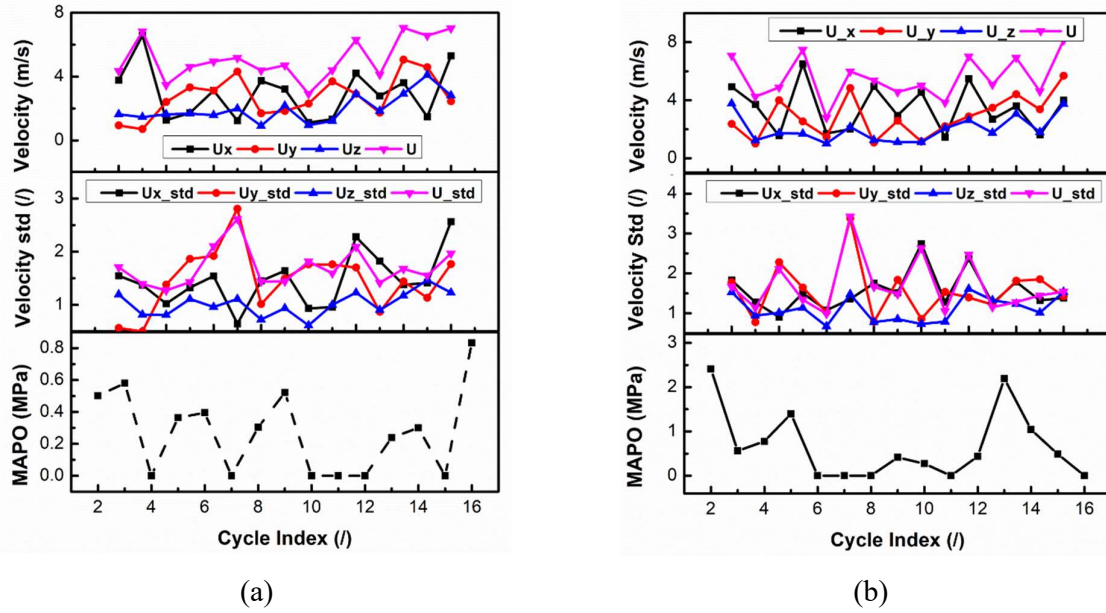


Fig. 7. The magnitude and standard deviation of velocity at the spark plug for LES cycles under the (a) mild knock and (b) heavy knock conditions.

To sum up, the cycle with intensive pressure oscillations had a higher peak pressure, and this positive correlation was found to be stronger under the heavy knock condition, however, a clear linear relationship seems to not exist between knock intensity and combustion phasing and the flow near the sparkplug. The results illustrate that the formation of strong pressure oscillation depends on the local evolution of the flow field under a certain operating condition. To explain the positive or negative relationship between the combustion indicators mentioned above, and further explore the combustion process for different knock intensities, detailed analysis of 3-D LES results was conducted. The findings are discussed in the next section.

4.3. Pressure oscillation formation in representative cycles

Figure 8(a) presents the pressure traces of two cycles (cycle 2 and cycle 5) with strong knock intensity and cycle 12 with mild knock intensity. It implies that cycle 2 has the fastest flame propagation speed, since the pressure rises more quickly than for cycle 5 and cycle 12. Moreover, the pressure

fluctuations in cycle 2 occur earlier than in cycle 5 and cycle 12. It is noticeable that the pressure oscillation reaches its highest amplitude once the fluctuation occurs in cycle 5, however, there is an obvious process of enhancement in the amplitude for cycle 2. Figure 8(b) illustrates the corresponding profiles of heat release rate versus crank angle. A quick heat release caused by the auto-ignition of the end gas can be seen during the knocking combustion. Although the MAPO of cycle 5 is less than that of cycle 2, the peak value of heat release rate in cycle 5 is higher. On the other hand, cycle 12 has a retarded and relatively lower heat release rate peak.

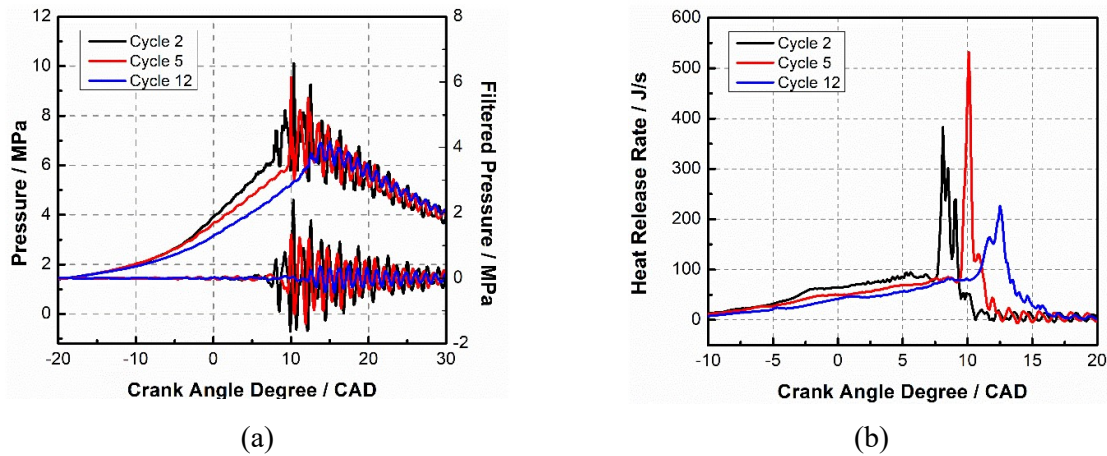


Fig. 8. (a) The original and filtered pressure inside the cylinder and (b) the heat release rate, for cycles 2, 5 and 12 under the heavy knock condition.

Figure 9 compares the flame front location and spatial distributions of temperature, velocity and equivalence ratio on the plane of $Z = -5.0$ mm just before the auto-ignition of end gas mixture. As shown, the inhomogeneity in both temperature and equivalence ratio are prevalent in the unburnt mixture, and the end gas temperature of cycle 12 is relatively low.

Figure 10 shows the development of auto-ignition kernels and propagation of pressure waves (represented by the pressure difference, ΔP) for cycle 2 during the knocking combustion process. At 7.7 CAD aTDC, three auto-ignition kernels occur simultaneously. Two of them which are closer to

the flame front develop very fast and a local pressure pulse is induced consequently at 7.8 CAD aTDC. The pressure wave propagating towards the burnt mixture decays due to dissipation, however, the pressure wave is enhanced by the chemical heat release along the unburnt mixture near the cylinder wall.

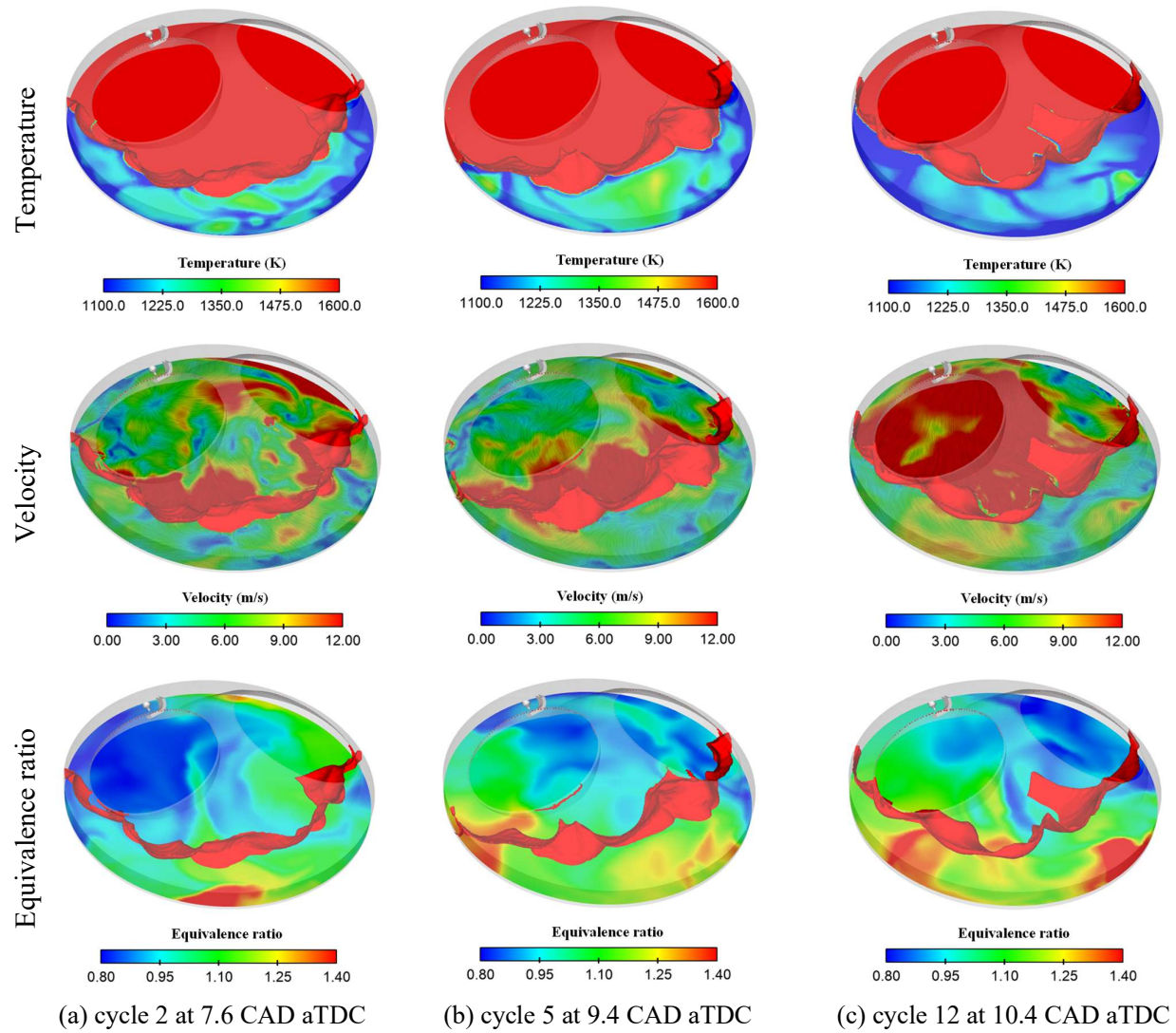
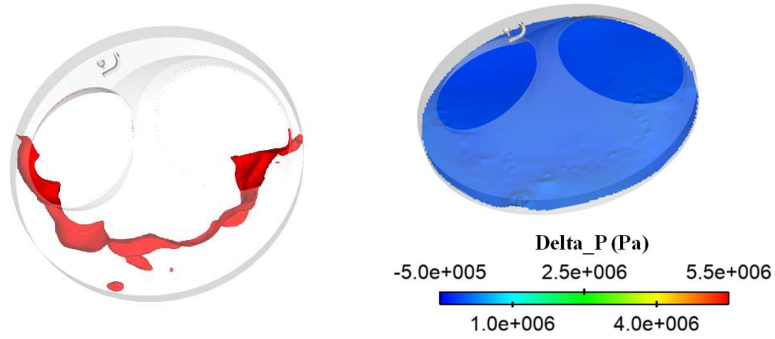
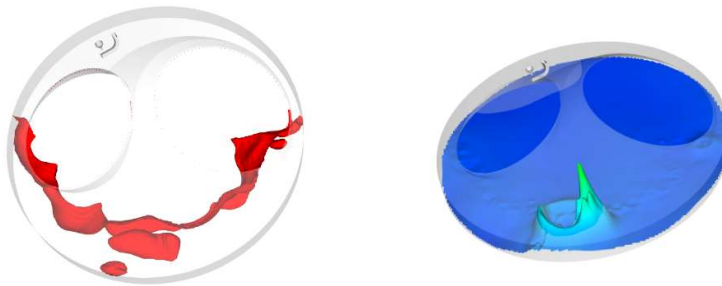


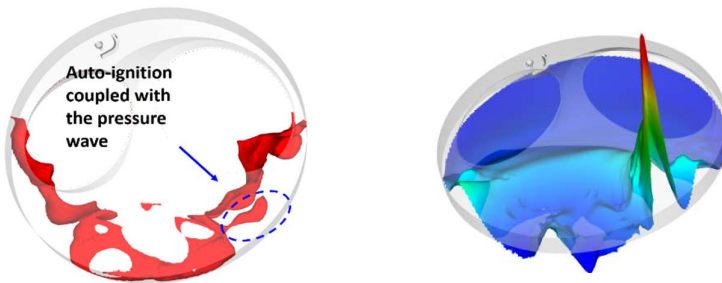
Fig. 9. The temperature, velocity and equivalence ratio spatial distributions at the crank angle just before auto-ignition, (a) 7.6 CAD aTDC of cycle 2, (b) 9.4 CAD aTDC of cycle 5, (b) 10.4 CAD aTDC of cycle 12. The iso-surface of temperature = 1600.0 K represents the flame front.



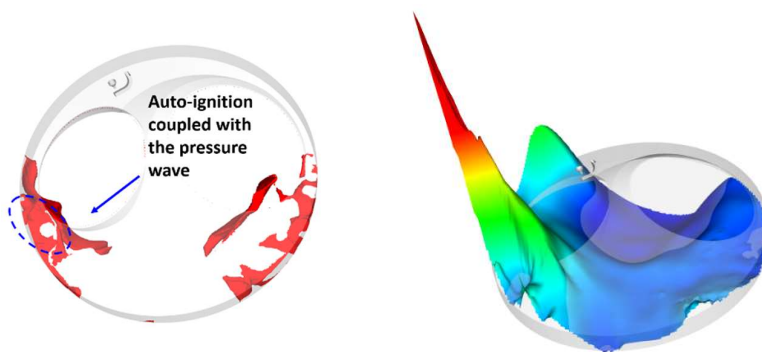
7.7 CAD aTDC



7.8 CAD aTDC



8.2 CAD aTDC



9.1 CAD aTDC

Fig. 10. The evolution of auto-ignition kernel development (left) and propagation of pressure waves (right) during the knocking combustion process of cycle 2 under heavy knock condition. On the left figures, the iso-surface correspond to $T = 1600.0$ K.

Moreover, being compressed by the pressure wave, new spontaneous kernels are generated, the quick local heat release, in turn intensifies the pressure wave, and the coupling between pressure and chemical reaction waves forms a strong pressure peak as seen at 8.2 CAD aTDC and 9.1 CAD aTDC. Since several new auto-ignition kernels generate consequently on the right side of the original spontaneous spots (at 7.7 CAD aTDC), the most intensive pressure wave spreads counterclockwise along the cylinder wall during the combustion process of cycle 2.

In addition, we compared the local pressure profiles at different locations inside the combustion chamber. The 24 monitor points are located in two X-Y planes as shown in Fig. 11. The location of the monitor point at the same position as the pressure sensor in experiments is labeled 3.0_0.

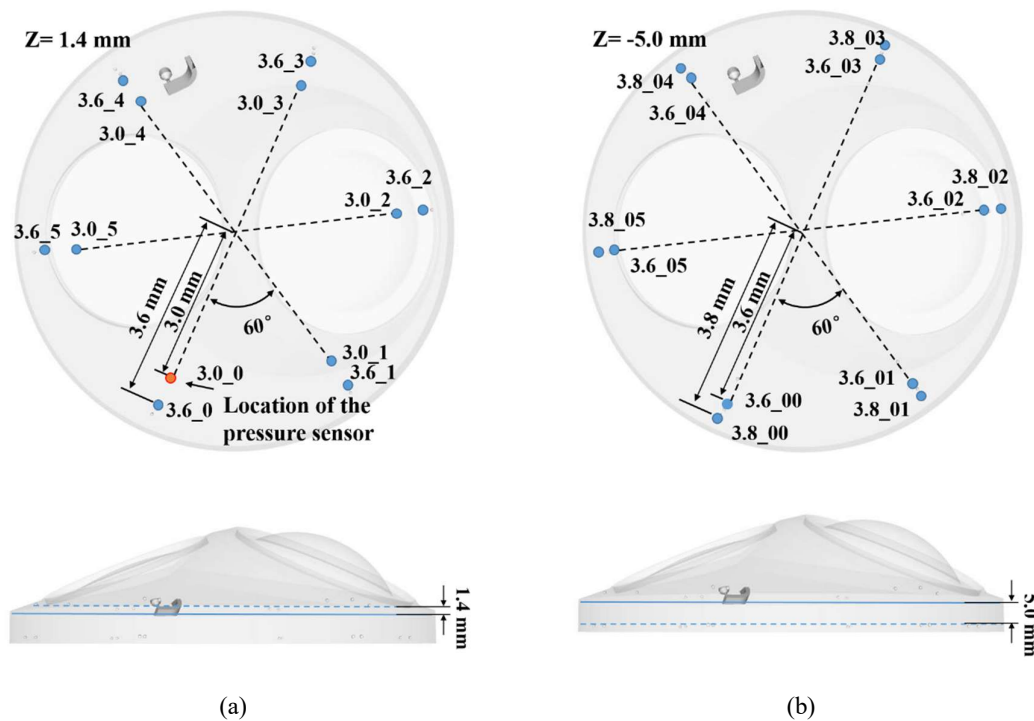


Fig. 11. The location of monitor points in the combustion chamber: (a) on the Z=1.4 mm plane; (b) on the Z=-5.0 mm plane.

As shown in Figure 12, the onset of pressure oscillations follows the order from “*_0” to “*_5”, in the anti-clockwise direction. This can be explained by the fact that the strongest local pressure wave

propagates in that direction as mentioned above. Furthermore, the points near the cylinder wall have higher amplitude of fluctuation because the pressure wave is reinforced by the heat released due to chemical reactions in the end gas mixture. Since most of the auto-ignition kernels during the combustion of cycle 2 are generated closer to the piston rather than the top of combustion chamber, the points on the plane of $Z = -5.0$ mm have overall higher pressure oscillation amplitudes. Also, the results imply that the difference in pressure oscillations depends on the development of pressure wave during the combustion process.

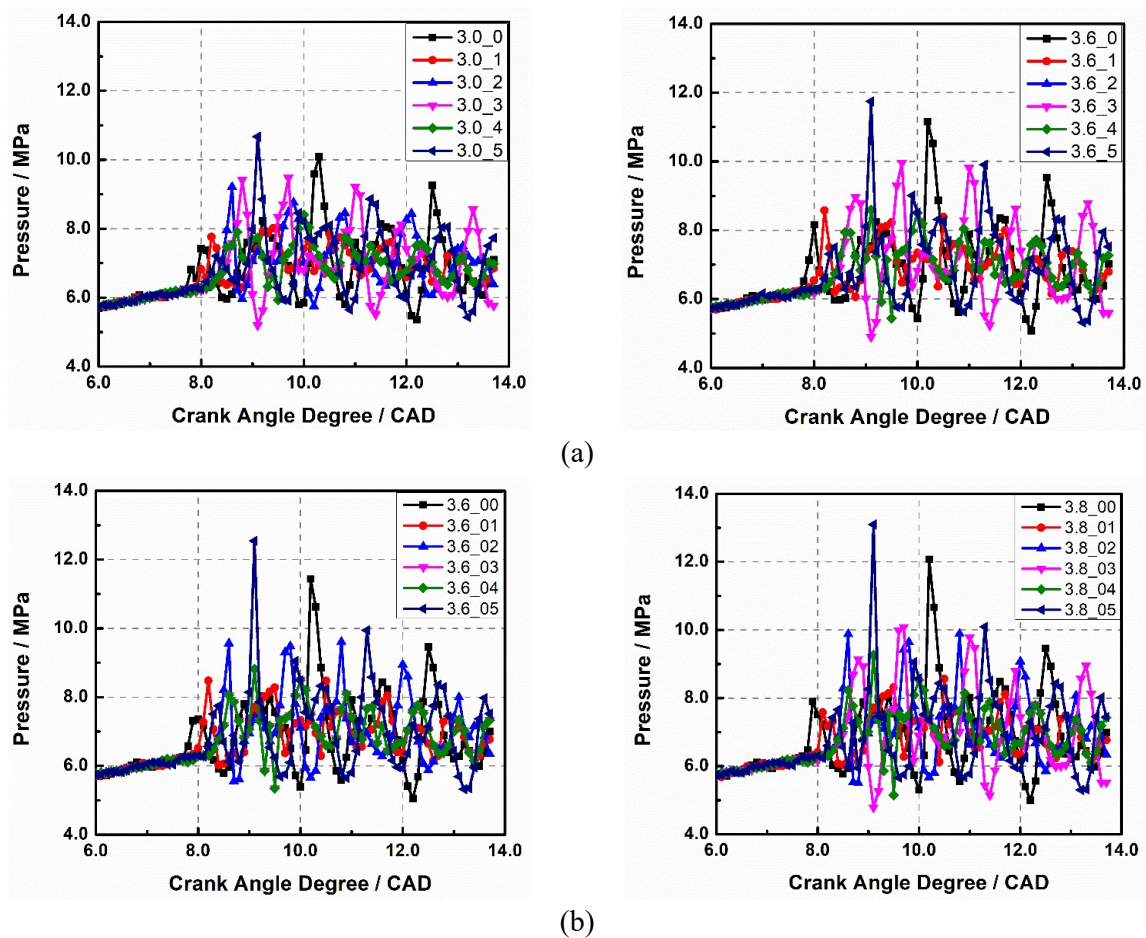


Fig. 12. The pressure profiles obtained from different monitor points in the combustion chamber: (a) monitor points on the $Z=1.4$ mm plane; (b) monitor points on the $Z=-5.0$ mm plane of cycle 2 under

heavy knock condition.

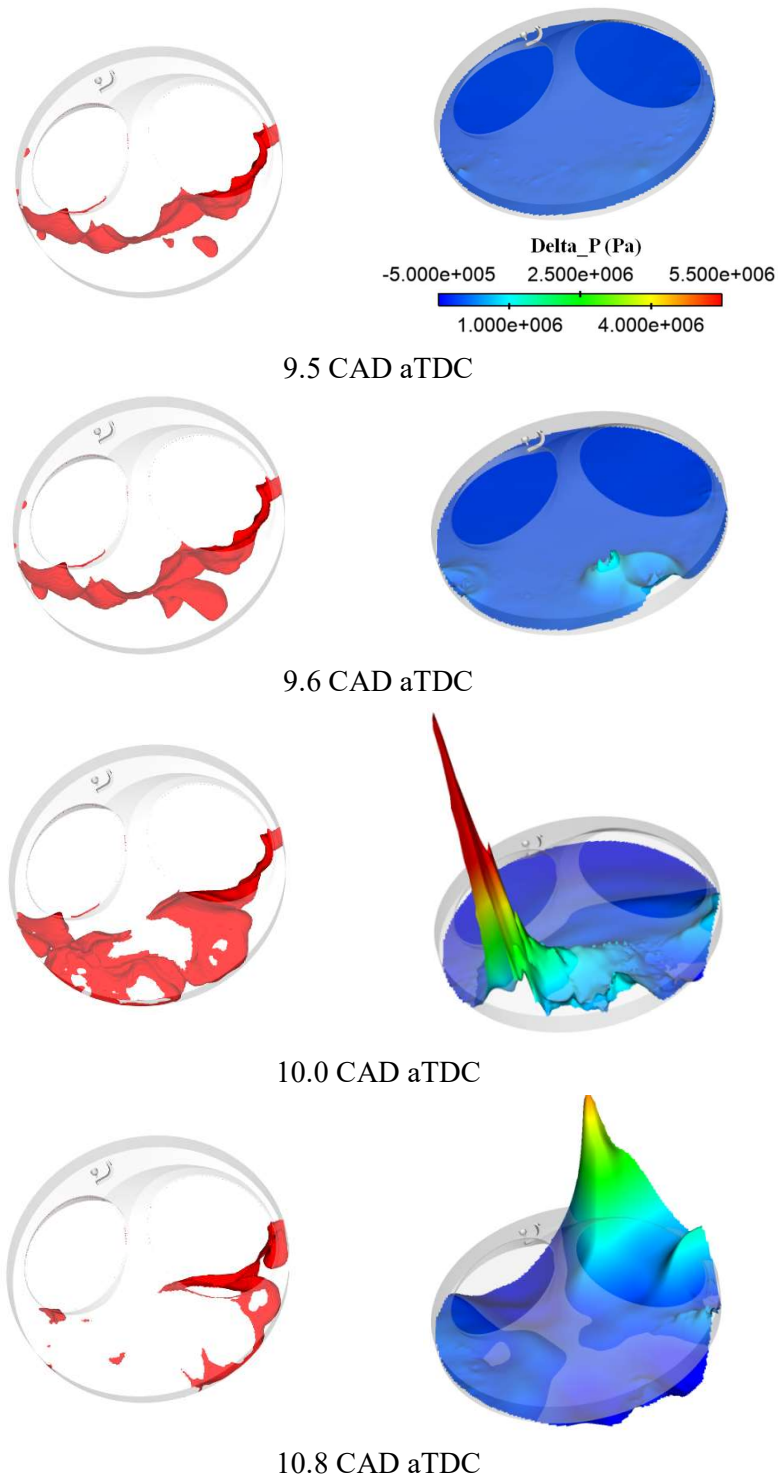


Fig. 13. The evolution of auto-ignition kernel development (left) and propagation of pressure wave (right) during the knocking combustion process of cycle 5 under the heavy knock condition. On the

left figures, the iso-surface correspond to $T = 1600.0$ K.

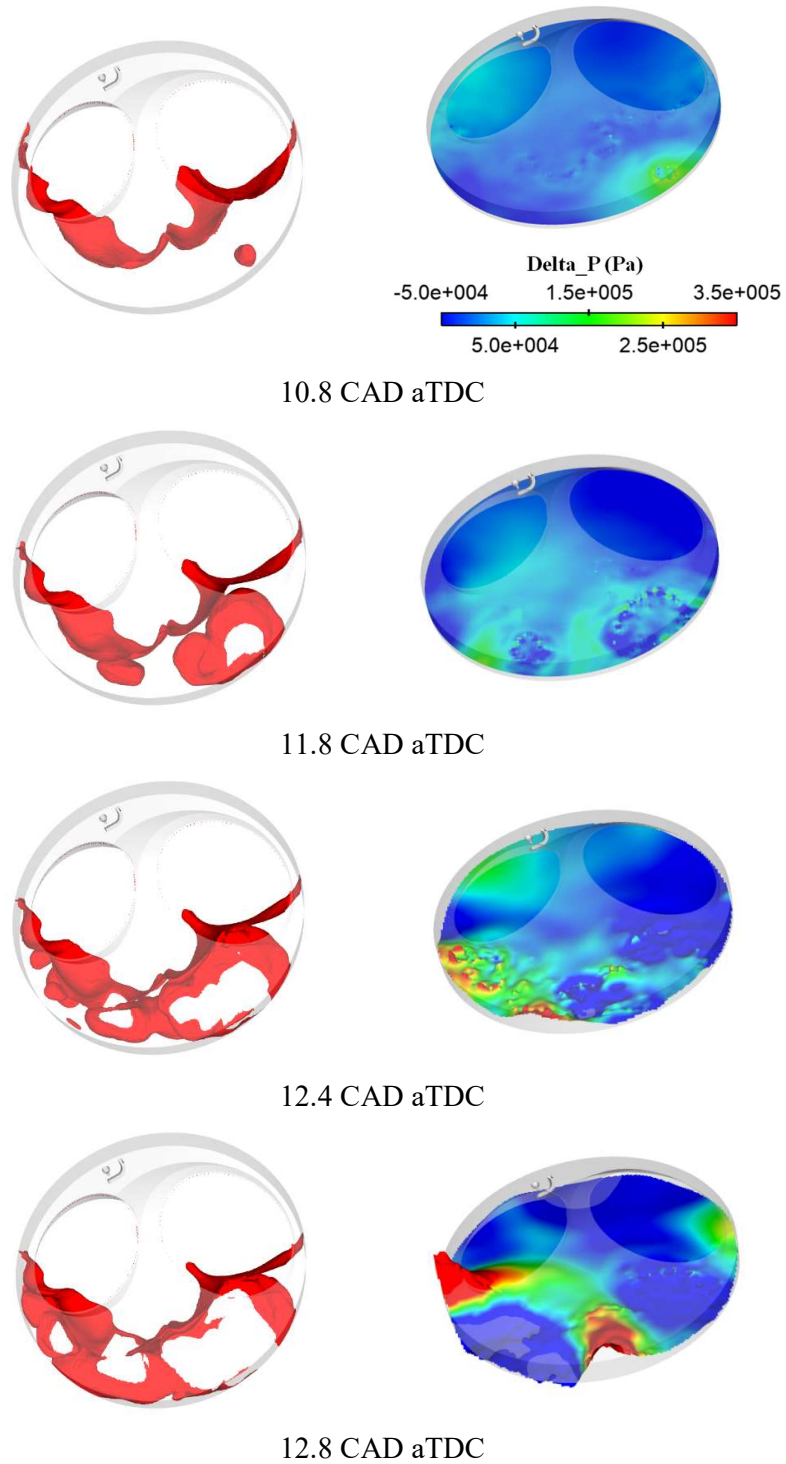


Fig. 14. The evolution of auto-ignition kernel development (left) and propagation of pressure wave (right) during the knocking combustion process of cycle 12 under the heavy knock condition. On the left figures, the iso-surface correspond to $T = 1600.0$ K.

Figure 13 shows the evolution of auto-ignition and pressure waves inside the cylinder during the knocking combustion of cycle 5. Multiple auto-ignition kernels occur at 9.5 CAD aTDC. Similar to the combustion process of cycle 2, the strongest pressure wave is induced by the coupling mechanism between the auto-ignition and pressure waves as shown for 10.0 and 10.1 CAD aTDC. As the piston moves downward, due to the effect of expansion, the latter formed auto-ignition kernel is not able to induce high pressure pulse at 10.8 CAD aTDC. During the combustion process, the most intensive pressure wave spreads clockwise along the cylinder wall.

Figure 14 illustrates the combustion process of cycle 12. As shown, there are still multiple spontaneous kernels occurring in the end gas mixture. However, since the development of the auto-ignition reaction front is slow, the probability of coupling between the reaction front and pressure wave becomes relatively low. As a result, the knock intensity is low.

As discussed above, the variation in knock intensity under abnormal combustion conditions can be large, and it is related to the coupling process between chemical heat release and pressure wave which can be influenced by the spatial distributions of the flow pattern, temperature and equivalence ratio in the end gas mixture. In addition, the present analyses are helpful to develop effective strategies to mitigate engine knock. For example, it is found that an early occurrence of auto-ignition in the end gas is prone to high knock intensity. Therefore, in a practical engine operating condition, it is important to suppress the early occurrence of auto-ignition. Potential strategies could be: reducing the chemical reactivity of the end-gas mixture by introducing partial lean mixture using multi-injection strategy; decreasing the inhomogeneity in the end gas region by strengthening the turbulence, in this way, the early occurrence of auto-ignition could be delayed as shown in our previous study [9], and the knock intensity could be reduced as illustrated in the present work. Furthermore, the effects of other factors,

such as manufacturing tolerances and spray process, would be conducted in the future work.

5. Conclusions

In this work, large-eddy simulation of a direct-injection spark-ignition engine were performed under operating conditions corresponding to varying levels of knock. The turbulence-chemistry interaction during premixed combustion was incorporated by using the level set G-Equation model. A toluene primary reference fuel mechanism was adopted to describe the auto-ignition in the end gas. The experimental pressure envelope was well reproduced by the LES, and both the averaged and variation coefficient values of knock intensity (represented by the maximum amplitude of pressure oscillation) were predicted with good accuracy.

Thereafter, a correlation analysis was conducted based on the combustion phasing, peak pressure and MAPO. The results shows that the cycle with intensive pressure oscillations had a higher peak pressure, and this positive correlation was found to be stronger under the heavy knock condition. To further explore the mechanism, a three dimensional spatial analysis for cycles with relatively stronger knock intensities and a cycle with mild knock intensity was conducted. From three dimensional analysis, it was shown that the coupling between multiple auto-ignition kernels and pressure and chemical reaction induced the higher pressure pulse and the subsequent strong pressure oscillation intensity. The pressure wave propagating towards the burnt mixture decayed due to dissipation. However, the pressure wave could be enhanced by the chemical heat release along the unburnt mixture near the cylinder wall. Moreover, being compressed by the pressure wave, new spontaneous kernels were formed, the quick local heat release in turn intensified the pressure wave, and the coupling between pressure and chemical reaction formed a strong pressure peak. Although multiple auto-ignition kernels could be found during the knocking combustion in different cycles, the degree of coupling between chemical reaction and

pressure wave varied, which led to variations in the knock intensity.

In addition, the relationship among knock intensity, onset of knock, combustion phasing and magnitude of flow velocity and standard deviation of flow velocity near the spark plug close to the ignition timing was also analyzed. It turns out that the correlations are relatively low. The knock intensity did not show a clear linear relationship with combustion phasing and the flow near the spark plug. The results illustrate that the formation of strong pressure oscillations depends on the local evolution of heat release and coupling between pressure and combustion. However, we could still explain the positive or negative relationship between them after conducting the three dimensional analysis. For example, an early occurrence of pressure oscillation (early auto-ignition occurrence) was more prone to high knock intensity, the reason is the chemical reactivity of ending gas is much higher near the TDC (usually with higher pressure and temperature). The pressure wave propagating towards the burnt mixture could be easier to be enhanced by the heat released from the ending gas. Moreover, a faster flame propagation could be induced by the coupling between multiple auto-ignition kernels and pressure and chemical reaction, therefore, the cycle with heavy knock could usually have short combustion duration. Analyses such as these are helpful to get a detailed understanding of the link between cycle-to-cycle variation and knock intensity, which can be utilized to develop effective strategies to mitigate engine knock.

Acknowledgments

The submitted manuscript has been created by UChicago Argonne, LLC, Operator of Argonne National Laboratory (Argonne). Argonne, a U.S. Department of Energy Office (DOE) of Science laboratory, is operated under Contract No. DE-AC02- 06CH11357. The U.S. Government retains for itself, and others acting on its behalf, a paid-up nonexclusive, irrevocable worldwide license in said

article to reproduce, prepare derivative works, distribute copies to the public, and perform publicly and display publicly, by or on behalf of the Government.

This work has been supported by the National Science Fund for Distinguished Young Scholars (No. 51825603), the experimental data are from Tianjin University, China. Argonne National Laboratory's work was supported by the U.S. Department of Energy, Office of Energy Efficiency and Renewable Energy, Vehicle Technologies Office under contract DE-AC02-06CH11357.

We gratefully acknowledge the computing resources provided on Blues, a high-performance computing cluster operated by the Laboratory Computing Resource Center (LCRC) at Argonne National Laboratory. The authors also thank Dr. Sameera Wijeyakulasuriya from Convergent Science Inc. for his valuable inputs and feedback with regard to the engine LES study.

References

- [1] Kalghatgi GT. Developments in internal combustion engines and implications for combustion science and future transport fuels. *Proc Combust Inst.* 2015;35:101-15.
- [2] Kalghatgi G, Levinsky, H., Colket, M. Future transportation fuels. *Prog Energy Combust Sci.* 2018;69:103-5.
- [3] De Bellis V. Performance optimization of a spark-ignition turbocharged VVA engine under knock limited operation. *Appl Energy.* 2016;164:162-74.
- [4] Pan M, Wei H, Feng D, Pan J, Huang R, Liao J. Experimental study on combustion characteristics and emission performance of 2-phenylethanol addition in a downsized gasoline engine. *Energy.* 2018;163:894-904.
- [5] Zhen X, Wang Y, Xu S, Zhu Y, Tao C, Xu T, Song M. The engine knock analysis—An overview. *Appl Energy.* 2012;92:628-36.
- [6] Wang Z, Qi Y, He X, Wang J, Shuai S, Law CK. Analysis of pre-ignition to super-knock: hotspot-induced deflagration to detonation. *Fuel.* 2015;144:222-7.
- [7] Vafamehr H, Cairns A, Sampson O, Koupaie MM. The competing chemical and physical effects of transient fuel enrichment on heavy knock in an optical spark ignition engine. *Appl Energy.* 2016;179:687-97.
- [8] Heywood JB. *Internal combustion engine fundamentals* 1988.
- [9] Wei H, Chen C, Zhou H, Zhao W, Ren Z. Effect of turbulent mixing on the end gas auto-ignition of n-heptane/air mixtures under IC engine-relevant conditions. *Combust Flame.* 2016;174:25-36.
- [10] Zeldovich YB. Regime classification of an exothermic reaction with nonuniform initial conditions. *Combust Flame.* 1980;39:211-4.
- [11] Gu X, Emerson D, Bradley D. Modes of reaction front propagation from hot spots. *Combust Flame.* 2003;133:63-74.
- [12] Pal P. *Computational Modeling and Analysis of Low Temperature Combustion Regimes for Advanced Engine Applications* 2016.
- [13] Pal P, Valorani M, Arias PG, Im HG, Wooldridge MS, Ciottoli PP, Galassi RM. Computational characterization of ignition regimes in a syngas/air mixture with temperature fluctuations. *Proc Combust Inst.* 2017;36:3705-16.
- [14] Dai P, Chen Z, Chen S, Ju Y. Numerical experiments on reaction front propagation in n-heptane/air mixture with temperature gradient. *Proc Combust Inst.* 2015;35:3045-52.
- [15] Terashima H, Koshi M. Mechanisms of strong pressure wave generation in end-gas autoignition during knocking combustion. *Combust Flame.* 2015;162:1944-56.
- [16] Pan J, Sheppard C. A theoretical and experimental study of the modes of end gas autoignition leading to knock in SI engines. *SAE transactions*; 1994. p. 1925-47.
- [17] Wei H, Chen C, Shu G, Liang X, Zhou L. Pressure wave evolution during two hotspots autoignition within end-gas region under internal combustion engine-relevant conditions. *Combust Flame.* 2018;189:142-54.
- [18] Yoo CS, Lu T, Chen JH, Law CK. Direct numerical simulations of ignition of a lean n-heptane/air mixture with temperature inhomogeneities at constant volume: Parametric study. *Combust Flame.* 2011;158:1727-41.
- [19] Yoo CS, Luo Z, Lu T, Kim H, Chen JH. A DNS study of ignition characteristics of a lean iso-octane/air mixture under HCCI and SACI conditions. *Proc Combust Inst.* 2013;34:2985-93.
- [20] Liang L, Reitz RD, Iyer CO, Yi J. Modeling knock in spark-ignition engines using a G-equation combustion model incorporating detailed chemical kinetics. *SAE Technical Paper*; 2007-01-0165.
- [21] Pal P, Wu Y, Lu T, Som S, See YC, Le Moine A. Multidimensional numerical simulations of knocking combustion in a cooperative fuel research engine. *J Energy Res Technol.* 2018;140:102205.
- [22] Netzer C, Seidel L, Pasternak M, Lehtiniemi H, Perlman C, Ravet F, Mauss F. Three-dimensional computational fluid dynamics engine knock prediction and evaluation based on detailed chemistry and detonation theory. *Int J Eng Res* 2018;19:33-44.

- [23] Bates L, Bradley D. Deflagrative, auto-ignitive, and detonative propagation regimes in engines. *Combust Flame*. 2017;175:118-22.
- [24] D'Adamo A, Breda S, Fontanesi S, Irimescu A, Merola SS, Tornatore C. A RANS knock model to predict the statistical occurrence of engine knock. *Appl Energy*. 2017;191:251-63.
- [25] Ameen MM MM, Millo F, Som S. Numerical prediction of cyclic variability in a spark ignition engine using a parallel large eddy simulation approach. *J Energ Resour-ASME*. 2018;140 052203.
- [26] Robert A, Richard S, Colin O, Martinez L, De Francqueville L. LES prediction and analysis of knocking combustion in a spark ignition engine. *Proc Combust Inst*. 2015;35:2941-8.
- [27] Vermorel O, Richard S, Colin O, Angelberger C, Benkenida A, Veynante D. Multi-cycle LES simulations of flow and combustion in a PFI SI 4-valve production engine. *SAE Technical Paper*; 2007-01-0151.
- [28] Colin O, Cruz APD, Jay S. Detailed chemistry-based auto-ignition model including low temperature phenomena applied to 3-D engine calculations. *Proc Combust Inst*. 2005;30:2649-56.
- [29] Pan J, Wei H, Shu G, Pan M, Feng D, Li N. LES analysis for auto-ignition induced abnormal combustion based on a downsized SI engine. *Appl Energy*. 2017;191:183-92.
- [30] Robert A, Truffin, K., Iafrate, N., Jay, S., Colin, O. and Angelberger, C. Large-eddy simulation analysis of knock in a direct injection spark ignition engine. *Int J Engine Res*. 2019;20:765-76.
- [31] GT-Power User's Manual GT-Suite™ Version 6.1. Gamma Technologies; 2004.
- [32] Leguille M, Ravet F, Le Moine J, Pomraning E, Richards K, Senecal P. Coupled Fluid-Solid Simulation for the Prediction of Gas-Exposed Surface Temperature Distribution in a SI Engine. *SAE Technical Paper*; 2017-01-0669.
- [33] Richards K, Senecal P, Pomraning E. CONVERGE Manual-CONVERGE CFD 2.3. Madison, WI2016.
- [34] Beale JC, Reitz RD. Modeling spray atomization with the Kelvin-Helmholtz/Rayleigh-Taylor hybrid model. *Atomization Spray*. 1999;9.
- [35] Schmidt DP, Rutland C. A new droplet collision algorithm. *J Comput Phys*. 2000;164:62-80.
- [36] Pal P, Keum S, Im HGJJoER. Assessment of flamelet versus multi-zone combustion modeling approaches for stratified-charge compression ignition engines. 2016;17:280-90.
- [37] Chen C, Ameen MM, Wei H, Iyer C, Ting F, Vanderwege B, Som S. LES analysis on cycle-to-cycle variation of combustion process in a DISI engine. *SAE Technical Paper*; 2019-01-0006.
- [38] Metghalchi M, Keck JC, flame. Burning velocities of mixtures of air with methanol, isooctane, and indolene at high pressure and temperature. *Combust Flame*. 1982;48:191-210.
- [39] Pan M, Huang R, Liao J, Ouyang T, Zheng Z, Lv D, Huang H. Effect of EGR dilution on combustion, performance and emission characteristics of a diesel engine fueled with n-pentanol and 2-ethylhexyl nitrate additive. *Energ Convers Manage*. 2018;176:246-55.
- [40] Liu Y-D, Jia M, Xie M-Z, Pang B. Development of a new skeletal chemical kinetic model of toluene reference fuel with application to gasoline surrogate fuels for computational fluid dynamics engine simulation. *Energ Fuel*. 2013;27:4899-909.
- [41] Morgan N, Smallbone A, Bhave A, Kraft M, Cracknell R, Kalghatgi G. Mapping surrogate gasoline compositions into RON/MON space. *Combust Flame*. 2010;157:1122-31.
- [42] Fraser N, Blaxill H, Lumsden G, Bassett M. Challenges for increased efficiency through gasoline engine downsizing. *SAE Int J Engines*2009. p. 991-1008.
- [43] Yu H, C. Qi, Z. Chen Effects of flame propagation speed and chamber size on end-gas autoignition. *Proc Combust Inst*. 2016.